Comparison of predicted and experimental DSC curves for vegetable oils

M. Teles dos Santos [a,b,*], V. Gerbaud [b], G.A.C. Le Roux [a]

[a] LSCP/CESQ – Department of Chemical Engineering, University of São Paulo, Av. Prof. Luciano Gualberto, 380, 05508-900 São Paulo, SP, Brazil
[b] LGC – INP ENSIACET, 4 Allée Emile Monso, 31030 Toulouse, France

A B S T R A C T

We compare experimental and predicted differential scanning calorimetry (DSC) curves for palm oil (PO), peanut oil (PeO) and grapeseed oil (GO). The predicted curves are computed from the solid–liquid equilibrium modelling and direct minimization of the Gibbs free energy. For PO, the lower the scan rate, the better the agreement. The temperature transitions of PeO and GO were predicted with an average deviation of −0.72 °C and −1.29 °C respectively, in relation to experimental data from literature. However, the predicted curves showed other peaks not reported experimentally, as computed DSC curves correspond to equilibrium hypothesis which is reached experimentally for an infinitely small scan rate. The results revealed that predicted transitions temperatures using equilibrium hypotheses can be useful in pre-experimental evaluation of vegetable oils formulations seeking for desired melting profiles.

Keywords:
Triacylglycerols
DSC
Solid–liquid equilibrium
Vegetable oil

1. Introduction

As the industrial usage of vegetables oils increases, the knowledge of thermal profile of such systems becomes fundamental, especially for product design purposes. The melting profile of a vegetable oil plays a fundamental role on product development, as the quantity of solid fat in a given temperature strongly influences the suitability of the fat for a particular application. We have recently used a predictive approach based on solid–liquid equilibrium (SLE) modelling and optimization tools to compute the melting curves of vegetable oils and their blends. It was validated for a large variety of systems composed by triacylglycerols (TAGs) molecules [1–4]. Moreover, SLE problem resolution also allows computing the Excess Gibbs free energy at a given temperature, which can then be used to compute the changes in heat capacity due to solid–liquid transitions. These theoretical changes in heat capacity can be also compared with experimental data, namely DSC curves. The objective of the present work is further comparing the predicted results with experimental data, specially the phase transition temperatures, analyzing the capability of the equilibrium based model in describe experimental DSC curves for vegetable oils.

It is known that experimental DSC curves are strongly influenced by many factors, such as heat/cooling scan rates, thermal lag and sample size. The predicted DSC curves of the present approach are, however, based on equilibrium hypotheses, which would correspond to an infinitely low scan rate.

2. Models

2.1. DSC calculations

DSC curves record the changes in heat capacity of a material as the temperature changes. The apparent heat capacity (due to phase transitions) is given by:

$$C_p^{ap} = \frac{\partial q_L}{\partial T} + \frac{\partial q_S}{\partial T} + \frac{\partial q_{SL}}{\partial T} \tag{1}$$

where q_L and q_S are, respectively, the specific heat consumed in raising the temperature of the solid and the liquid phase and ∂q_{SL} is the latent heat of melting at $T + 1/2\partial T$ (average melting temperature). As we are interesting in evaluating the temperatures where occur the solid–liquid transitions, we must evaluate the third term on right hand side of Eq. (1). Therefore:

$$C_{SL} \equiv \frac{\partial q_{SL}}{\partial T} = C_p^{ap} - \frac{\partial q_L}{\partial T} - \frac{\partial q_S}{\partial T} \tag{2}$$

C_{SL} represents the heat capacity due to the melting of TAGs and we are interested in its prediction. Considering that the reference liquid enthalpy is zero, the enthalpy of a pure molecule i on solid phase j ($H_{i,0}^{j}$) is equal to the melting enthalpy on this crystalline state j (ΔH_{melt}). Due to the non-ideal behavior on solid phase, the enthalpy

* Corresponding author at: LGC – INP ENSIACET, 4 Allée Emile Monso, 31030 Toulouse, France.
E-mail address: teles.msantos@gmail.com (M. Teles dos Santos).

of the solid mixture of triacylglycerols must take into account an Excess enthalpy. These considerations lead to:

$$H_{mix} = \sum_{j=1}^{np}\sum_{i=1}^{nc} n_i^j \Delta H_{melt\,i}^j + H^E \tag{3}$$

where n_i^j is the number of moles of component i on solid j, np is the number of phases and nc the number of components (TAGs). Eq. (3) represents the heat that must be provided to the solid sample to melt it (latent heat of melting).

By definition:

$$G^E = H^E - TS^E \tag{4}$$

Considering the solid mixtures of triacylglycerols as regular solutions ($S^E = 0$) and using Eq. (4) on Eq. (3), the final expression for the apparent heat capacity due to solid–liquid transitions becomes:

$$C_{SL} = \frac{\partial G^E}{\partial T} + \sum_{j=1}^{np}\sum_{i=1}^{nc} \Delta H_{melt\,i}^j \frac{\partial n_i^j}{\partial T} \tag{5}$$

Eq. (5) shows that for each point in a DSC curve, the apparent heat capacity due to solid–liquid transitions can be calculated using numerical derivatives of Excess Gibbs free energy and the number of mol of each molecule in each solid phase, evaluated at T_i and $T_i + \Delta T$. Those are computed from the SLE problem.

2.2. Solid–liquid equilibrium problem

In the present work, for a given temperature, a SLE problem is solved. Then, an increment in temperature is given, and the SLE problem is solved again in the new temperature. The variation in Excess Gibbs energy and the number of mol of each TAG that melt are recorded. Their numerical derivatives are finally used in Eq. (5) to predict a point in the calculated DSC curve.

2.2.1. SLE modelling

The intensive Gibbs energy for a phase j (g^j) is the weighted sum of the partial Gibbs energy of all components present in that phase. By definition, the partial Gibbs Energy of a component in a mixture is the chemical potential of that component in the mixture (μ_i^j). Therefore:

$$g^j = \sum_{i=1}^{nc} x_i^j(\mu_i^j) \Rightarrow g^j = \sum_{i=1}^{nc} x_i^j(\mu_{i,0}^j + RT\ \ln\ \gamma_i^j x_i^j) \tag{6}$$

where γ_i^j and x_i^j are the activity coefficient and molar fraction of component i on phase j, respectively, and $\mu_{i,0}^j$ is the chemical potential of pure component i at the same conditions (T,P) of the mixture.

For j = liquid:

Considering, as in our previous work [3], that the liquid phase is ideal, Eq. (6) is simplified to:

$$g^{liquid} = RT\sum_{i=1}^{nc}(x_i^{liquid}\ \ln\ x_i^{liquid}) \tag{7}$$

For j = solid:

The chemical potential of a pure component i in the solid state j in the temperature of the mixture (T) is given by [5]:

$$\mu_{i,0}^{solid(j)} = T\Delta H_{m,i}^{solid(j)}\left(\frac{1}{T_{m,i}^{solid(j)}} - \frac{1}{T}\right) \tag{8}$$

where $\Delta H_{m,i}^{solid(j)}$ and $T_{m,i}^{solid(j)}$ are, respectively, the melting enthalpy and melting temperature of TAG i on solid state j. Using Eq. (8) on Eq. (6), one have for the solid phases:

$$g^{solid(j)} = RT\sum_{i=1}^{nc} x_i^{solid(j)}\left(\frac{\Delta H_{m,i}^{solid(j)}}{R}\left(\frac{1}{T} - \frac{1}{T_{m,i}^{solid(j)}}\right) + \ln(\gamma_i^{solid(j)} x_i^{solid(j)})\right) \tag{9}$$

Three main possible solid states (polymorphic forms) are considered for TAGs: α, β' or β. Activity coefficients are needed to compute Gibbs free energy on solid states (Eq. (9)). The definition of activity coefficient is given by:

$$RT\ \ln\ \gamma_i(T,P,x) = \bar{g}_i^E = \left(\frac{\partial n g^E}{\partial n_i}\right)_{T,P,n_{j\neq i}} \tag{10}$$

So, an Excess Gibbs energy model must be used. The 2-sufixe Margules model was chosen for three main reasons: (1) it is suitable for mixtures where the components have similar molar volume, shape and chemical nature [5]; (2) an experimental database in TAGs is available allowing compute the model parameters [6] and it allows flexibility/simplicity required in the optimization step. The 2-sufixe Margules equation for multicomponent mixtures is given by:

$$g^E = \sum_{i=1}^{nc}\sum_{j=i+1}^{nc} A_{ij}x_i x_j \tag{11}$$

$$A_{ij} = 2qa_{ij} \tag{12}$$

The parameter q is a measure of molecular size in the considered pair (i,j) and x_i is the molar composition of TAG i. The parameters a_{ij} are related to interactions between TAGs i and j [5].

The necessary binary interaction parameters (A_{ij}) are calculated using correlations with the isomorphism between the two triacylglycerols i and j [6]. Once the activity coefficients are calculated, the Gibbs energy in each phase can be calculated using Eq. (7) or (9). Moreover, we use correlations to compute the melting temperature $T_{m,i}^{solid(j)}$ and melting enthalpy $\Delta H_{m,i}^{solid(j)}$ of each TAG in each crystalline state ($j = \alpha$, β' or β) [6,7]. As the TAG composition of the vegetable oil is an input, computing the Gibbs free energy of each phase becomes fully predictive.

2.2.2. Minimization of Gibbs free energy function

Solid–liquid phase equilibrium problem at a given temperature and pressure is the solution of a nonlinear programming (*NLP*) problem searching for the global minimization of the total Gibbs free energy subject to material balance constraints. Results provide the equilibrium distribution of each TAG among the solid and liquid phases. The problem can be stated as:

$$\min\ G(n) = \sum_{i=1}^{nc}\sum_{j=1}^{np} n_i^j \mu_i^j(n) = \sum_{j=1}^{np} n^j g^j \tag{13}$$

s.t.:

$$n_i = \sum_{j=1}^{np} n_i^j \quad i = 1 \ldots nc \tag{14}$$

$$0 \le n_i^j \le n_i \quad i = 1 \ldots nc; \quad j = 1 \ldots np \tag{15}$$

For a given composition in each phase, the activity coefficients are calculated and then, used to calculate the total Gibbs energy. The objective of the optimization step is determining the compositions of liquid and solid phases that minimize the total Gibbs energy

in a given temperature. For solve this Non Linear Programming problem, it was used a program developed in GAMS [8] using a Generalized Reduced Gradient (GRG)-based method.

3. Experimental data

3.1. Palm oil DSC

The DSC analysis was carried out using a DSG 60 equipment coupled with a FC-60-A (Shimadzu) and liquid nitrogen as cooling medium. The DSC instrument was calibrated with indium, zinc and lead. A palm oil sample of 9.7 mg was loaded into a standard aluminum pan and cover was hermetically sealed using manufacturer's crimping tool. An empty and hermetically sealed aluminum pan was used as reference. Firstly, the palm oil sample was heated to 80 °C and held for 5 min at this temperature. This is 2 times the final melting point of palm oil (approximately 40 °C) and it allows eventual crystal memory to be destroyed. The sample was then cooled from 80 °C to −50 °C and held at this temperature for 10 min. The sample was then reheated from −50 °C to 80 °C and the melting peaks were recorded. The samples were cooled and/or heated at two scanning rates: 5 °C min^{-1} and 10 °C min^{-1}.

3.2. Peanut oil and grapeseed oil DSC

The experimental DSC for these two systems was gathered from literature [9]. The temperature transitions predicted by the present work are then compared with the experimental peaks recorded at literature.

3.3. Triacylglycerols composition

For palm oil, the composition in terms of TAGs was taken from the literature [10]. For peanut oil and grapessed oil, the TAGs composition was computationally predicted in this work using the fatty acids data available [11], following the random distribution of fatty acids on glycerol structure to form triacylglycerols. Table 1 summarizes the TAG composition.

Table 1
Triacylglycerol composition of vegetable oils (% mass).

TAG	Palm oil[a] (%)	Peanut oil[b] (%)	Grapeseed oil[b] (%)
POO	22.43	6.85	–
POP	21.87	–	–
PPO	7.82	1.73	–
PPP	7.55	–	–
PLO	7.2	4.72	2.69
PLP	6.95	–	–
OOO	5.88	13.48	–
POS	3.82	–	–
POL	3.7	4.72	2.69
OPO	2.03	3.42	–
SOO	1.98	1.38	–
OOL	1.92	18.56	6.11
OLO	1.87	9.28	3.05
PPS	1.32	–	–
PPL	1.28	1.20	–
PLS	1.21	–	–
PLL	1.18	3.25	9.21
OLL	–	12.78	20.87
LOL	–	6.40	10.44
OPL	–	4.72	–
LLL	–	4.40	35.65
LPL	–	1.62	4.6
OOB	–	1.48	–
SLL	–	–	4.68

A triacylglycerol (TAG) is represented by its 3 fatty acids. P (palmitic C16:0); S (stearic C18:0); O (oleic C18:1), L (linoleic C18:2) and B (behenic C22:0).

[a] From literature.

[b] Predicted in this work.

4. Results and discussion

4.1. Palm oil

Fig. 1 shows the two experimental curves and the predicted one for palm oil, all of them carried out for the present work. As the output signal of the DSC experiments is in mW units and the predicted ones are kJ mol^{-1} K^{-1}, the 3 curves were normalized to obtain for the 3 cases an area under the curve equal to 1 (the temperatures transitions and shapes of the three curves remaining unchanged). The solid phase is assumed to be in crystalline state β', as palm oil is a β'-tending fat because of the presence of asymmetric mixed-acid TAGs, such as POO and PPO [12].

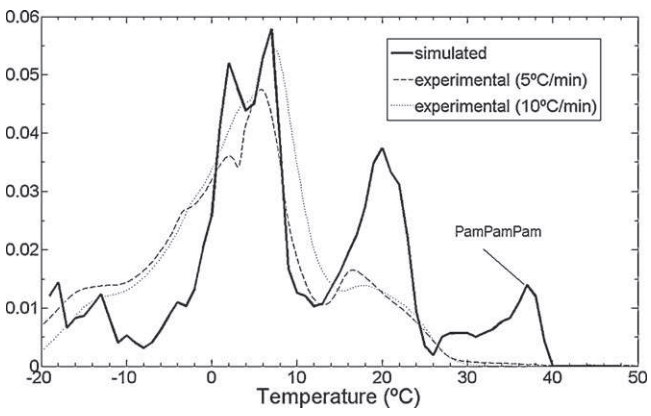

Fig. 1. Predicted and experimental DSC curves for a commercial palm oil sample. Pam: palmitic acid (C16:0).

The predicted distribution among the liquid and solid phases of the predominant molecules can be observed in Figs. 2–5.

Fig. 1 shows that the model was able to predict the two temperature ranges (0–10 °C and 15–25 °C) where the most pronounced phase transitions occur. These two regions correspond to the palm stearin (high melting fraction) and palm olein (low melting fraction), usually separated in industrial processing of palm oil. In addition, there is a steep decrease in heat capacity around 12 °C revealed by the two experimental curves and also correctly predicted by the present work.

However, two main differences arise from Fig. 1: the peak around 39 °C not present in the experimental curves and the range −15 °C to 0 °C.

The peak around 39 °C corresponds to the TAG PPP. A literature work [13] presents an experimental DSC for the palm oil with a heating rate of 1 °C min^{-1}, 5 °C min^{-1}, 10 °C min^{-1} and 20 °C min^{-1}. However, the authors observed a peak around 41.51 °C only when using the lowest scan rate (1 °C min^{-1}). That reinforced the previous discussion: the lower the scan rate, the closer to the equilibrium conditions, which are the ones used for predictions. At the equilibrium limit, there is a peak at 39 °C not detected using the higher heating scan rates (5 °C min^{-1} and 10 °C min^{-1}) used in this work.

The predicted DSC curves rely upon an equilibrium hypothesis, which means that chemical potentials are equal for all species in all phases. Said differently, the chemical potential difference is zero and there is no driving force for mass transfer between the liquid and solid phases. Experimentally, that would require infinitely low scan rates so that the system can reach equilibrium at each temperature point in the curve. This can explain the differences

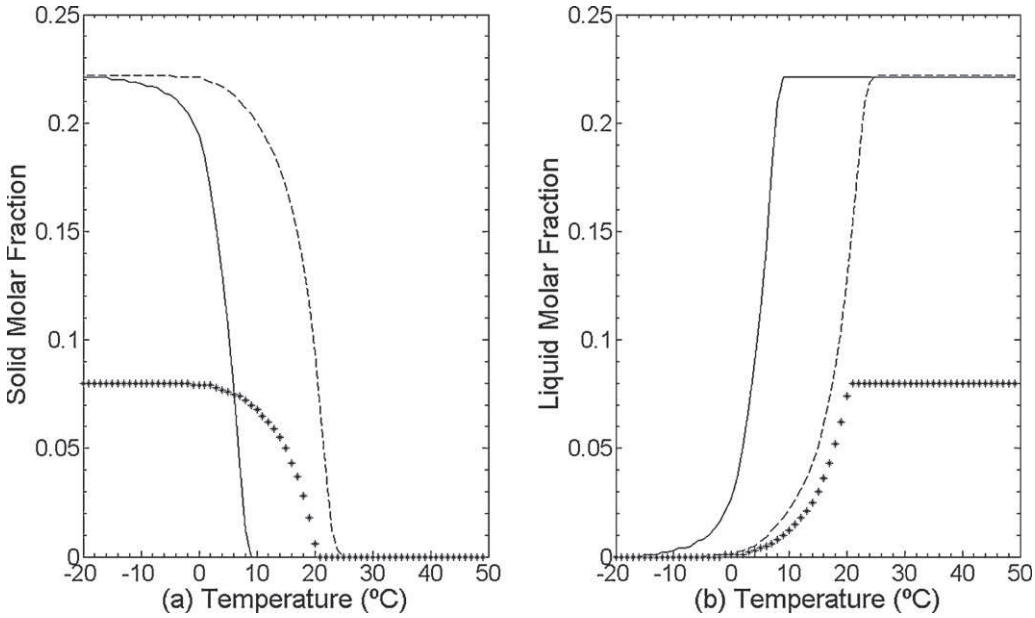

Fig. 2. Molar fraction in the solid phase (a) and liquid phase (b) of palm oil triacylglycerols. POO (—), POP (- - - -) and PPO (***).

between the predicted and experimental curves at the range −15 °C to 0 °C.

Also, it must be pointed out that the typical composition of palm oil used for DSC predictions (Table 1) and that from commercial oil used in DSC experiments (Fig. 1) can show some deviations.

The shape of the calculated curve in Fig. 1 is typical of mixtures with a large number of components: the number of peaks does not correspond to the number of chemical species (17), as TAGs melting over the same range lead to overlapping peaks. In order to better analyze this aspect, the temperature range of Fig. 1 was further analysed over 4 intervals: $T < 0\,^{\circ}C$, $0\,^{\circ}C \leq T \leq 10\,^{\circ}C$, $10\,^{\circ}C < T \leq 25\,^{\circ}C$ and $25\,^{\circ}C < T \leq 40\,^{\circ}C$. The fraction of each TAG on solid and liquid phases is shown in Figs. 2–5. One can observe the following solid–liquid transitions:

- $T < 0\,^{\circ}C$ (12 TAGs in solid–liquid transitions): POO, OOO, PLO, PLP, POL, OPO, SOO, OOL, OLO, PPL, PLS and PLL. All of them have mass fraction lower than 10%. The exception is POO (22.43%). However, this TAG is only at the beginning of its solid–liquid transition (Fig. 2). As all of the 11 others TAGs correspond to only 35.20% of palm oil, the 4 peaks at this range have relative low intensity. Figs. 2–5 show that most of those transitions occur over a temperature range, especially for POO, which starts melting at −16 °C and ends at +9 °C. One may attribute the first peak at −18 °C to the combined and fairly sharp transitions of OOO (−19 °C to −14 °C, Fig. 3), OOL (Fig. 4) and PLL (Fig. 5). The other three peaks (at −14 °C, −10 °C and −4 °C) are less easily assigned because the synergic effect of different solid–liquid transitions at this temperature ranges (Figs. 2–5).

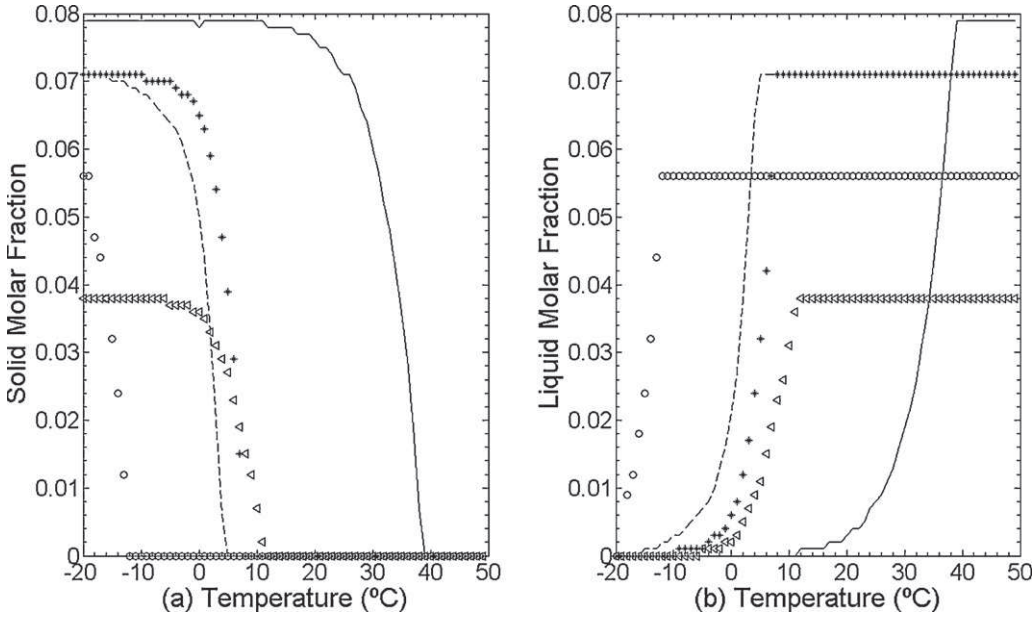

Fig. 3. Molar fraction in the solid phase (a) and liquid phase (b) of palm oil triacylglycerols. PPP (—), PLO (- - - -), PLP (***), OOO (◦) e POS (Δ).

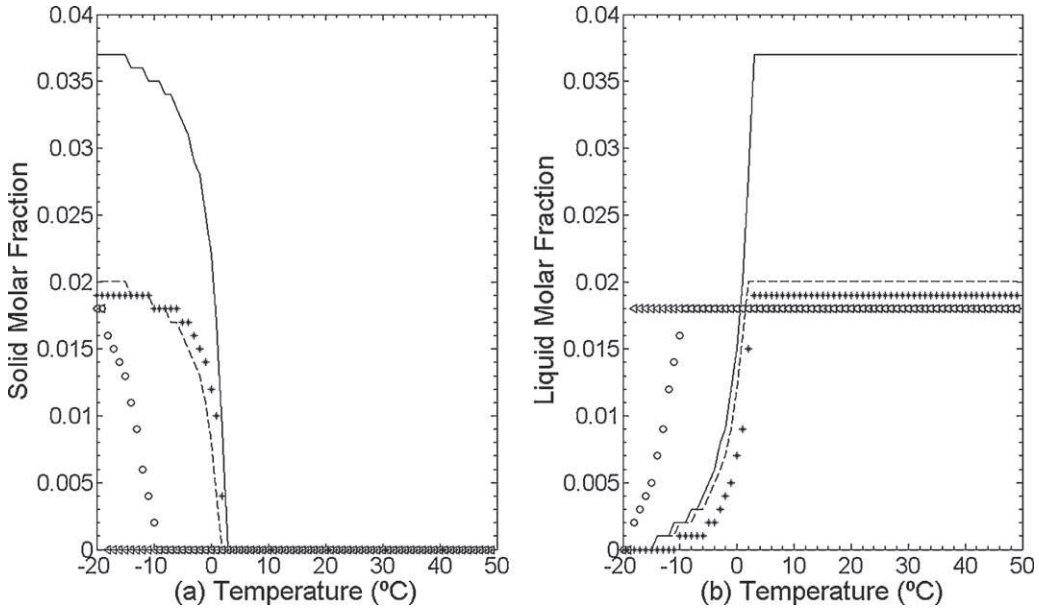

Fig. 4. Molar fraction in the solid phase (a) and liquid phase (b) of palm oil triacylglycerols. POL (—), OPO (- - - -), SOO (***), OOL (°) e OLO (Δ).

- $0\,^{\circ}C \leq T \leq 10\,^{\circ}C$ (10 TAGs in solid–liquid transitions): POO, POP, PPO, PLP, PLO, POS, OPO, SOO, POL and PLS. Some transition starts below 0 °C, like that of POO, but they end in this range. These explain the two peaks at +1.8 °C and +6.5 °C. The intensity is strong because the 10 TAGs melting in this range account for 79.01% in mass of the palm oil.
- $10\,^{\circ}C < T \leq 25\,^{\circ}C$ (5 TAGs in solid–liquid transitions): POP, PPO, PPP, POS and PPS. These TAGs are responsible for 42.38% of palm oil, corresponding to the second larger peak. A small bump at +12 °C can be related to the transition ending for POS. POP (21.87% in mass) and PPO (7.82% in mass) melt over this range. As their mass fraction is significant, a DSC peak occurs around +20.5 °C. Moreover, at this temperature range ($10\,^{\circ}C < T \leq 25\,^{\circ}C$), PPP and PPS start their transitions.
- $25\,^{\circ}C < T \leq 40\,^{\circ}C$ (2 TAGs in solid–liquid transitions): Over this range, only PPP and PPS are still in solid–liquid transitions (Figs. 3 and 5). A DSC rise occurs around +28 °C to 31 °C, likely due to the transition ending of PPS at +30 °C. At last, PPP ends its transition at +39 °C and causes the observed peak at this temperature.

The first compound among POO, POP and PPO to completely melt is POO (Fig. 2). This predicted result is in agreement with the fact that this is the compound with the lowest melting point, due to its higher degree of unsaturation (2 oleic chains).

Another interesting feature arising from the predicted results: there is a sharp difference on melting curves of POP and PPO, although these triacylglycerols are formed by the same fatty acids (palmitic and oleic). This highlights that the stereo-position of fatty acids must be taken into account when accessing properties such as melting enthalpy and melting point.

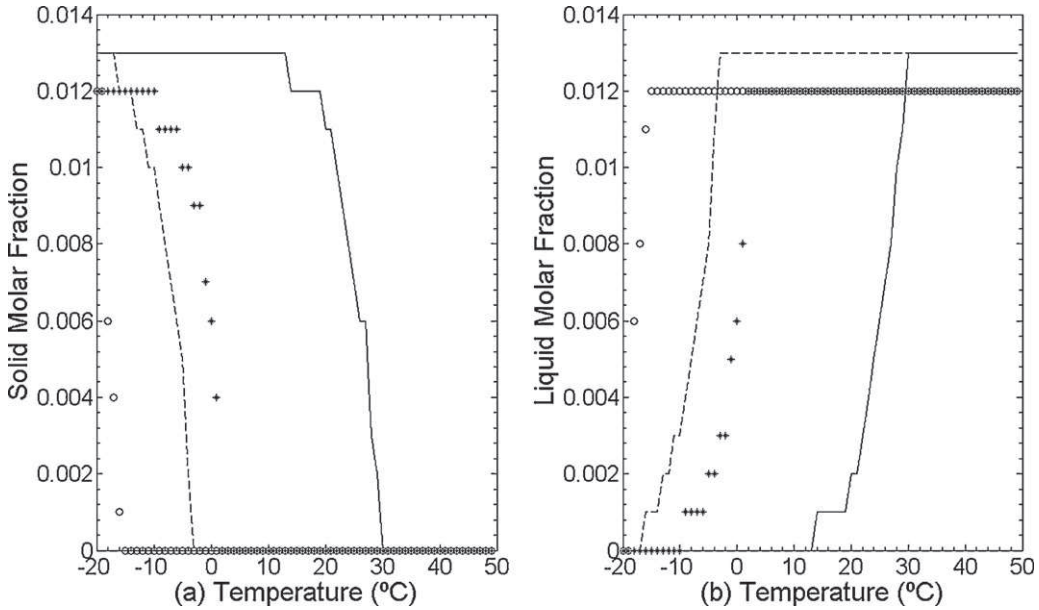

Fig. 5. Molar fraction in the solid phase (a) and liquid phase (b) of palm oil triacylglycerols. PPS (—), PPL (- - - -), PLS (***) e PLL (°).

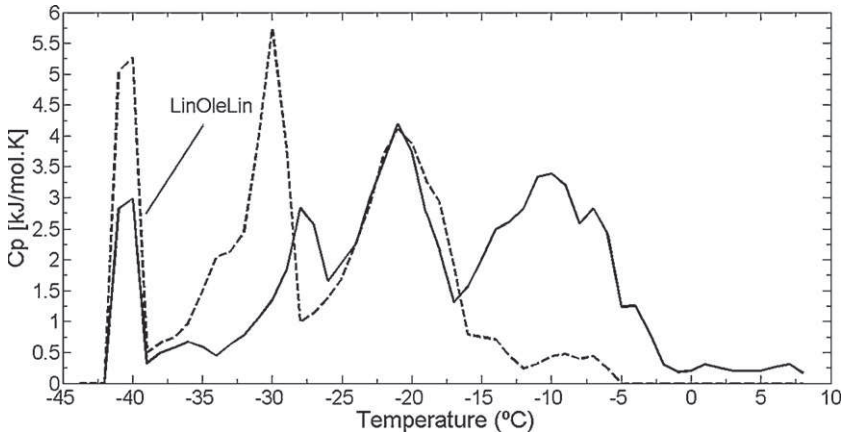

Fig. 6. Predicted DSC curve for peanut oil (full line) and grapeseed oil (dashed line).

Table 2
Experimental and calculated phase transitions DSC temperatures for peanut and grapeseed oil.

	Transition temperatures (°C)									
	Exp.	Calc.	Exp.	Calc.	Exp.	Calc.	Exp.	Calc.	Exp.	Calc.
Peanut oil	−51.7	nc	−29.7	−28	−14.57	−11	0.83	2	8.26	7
Grapeseed oil	−39.32	−40	−31.62	−30	−22.82	−21	−15.12	−15	–	–

nc: Not converged; Exp: experimental from [9]; Calc: calculated from this work.

4.2. Peanut and grapeseed oil

The predicted DSC curves for peanut oil and grapeseed oil are shown in Fig. 6. These oils have cosmetic, pharmaceutical and food applications.

It can be noted from Fig. 6 that the final melting point of grapessed oil is lower than that of peanut oil. This is due to the higher amount of unsaturated fatty acids in grapessed oil, which can be noted by its higher iodine value: 140.58 for grapessed oil and 95.23 for peanut oil [9]. In both oils, a sharp peak around −40 °C is observed. Further analyzing the fusion of each TAG separately, it corresponds to the TAG LOL. The other peaks cannot be unequivocally related to each TAG, because the transitions for each TAG do not occur in sharply distinguished temperature ranges and peaks overlap.

Table 2 shows the comparison of the transition temperatures observed in Fig. 6 and experimental ones from literature [9]. An average deviation of −0.72 °C and −1.29 °C were observed for peanut oil and grapeseed oil respectively. However, the predicted curves show other peaks not reported experimentally, due to the previously discussed reasons (equilibrium based model).

Unlike pure TAG, the polymorphic form of oils and fats cannot be established unequivocally by DSC and it can only be achieved by X-ray diffraction analysis. Therefore, polymorphic transformations in these two oils were not reported in the experimental literature study [9]. For calculations (Fig. 6), the oil is assumed to be crystallized on the β' form.

5. Concluding remarks

Solid–liquid phase transitions temperatures for palm oil, peanut oil and grapeseed oil could be predicted using thermodynamic equilibrium approach based on the optimization of Gibbs free energy. As the present method is predictive, it can be further used to pre-experimental evaluation of thermal profile of other vegetable oils and their blends. However, the shape of peaks on predicted DSC curves can be different from those of experimental ones, as experimental DSC is influenced by scan rate. In the first steps of product development, a useful task is to identify the temperatures in which the main phase transitions occur and determine the overall melting profile, rather than a detailed description of crystals. Taking into account this objective, the proposed approach to the problem revealed to be useful, despite the limitations of the model in not consider non-equilibrium states.

Acknowledgements

Authors would like to thank Mr. Omar J.G. Fernandéz for the valuable help during the development of the optimization code. In addition, we would also like to thank the financial support received from The National Council for Scientific and Technological Development (CNPq – Brazil), and the ALFA-II-400 FIPHARIA program (European Union).

References

[1] M. Teles dos Santos, G.A.C. Le Roux, X. Joulia, V. Gerbaud, Solid–liquid equilibrium modelling and stability tests for triacylglycerols mixtures, in: R.M.B. Alves, C.A.O. Nascimento, E. Biscaia (Eds.), Comput. Aid. Chem. Eng. 27 (2009) 885–890, http://dx.doi.org/10.1016/S1570-7946(09)70368-2.
[2] M. Teles dos Santos, G.A.C. Le Roux, V. Gerbaud, Computer-Aided Lipid Design: phase equilibrium modelling for product design, in: S. Pierucci, G. Buzzi Ferraris (Eds.), Comput. Aid. Chem. Eng. 28 (2010) 271–276, http://dx.doi.org/10.1016/S1570-7946(10)28046-X.
[3] M. Teles dos Santos, G.A.C. Le Roux, V. Gerbaud, Phase equilibrium and optimization tools application for enhanced structured lipids for foods, J. Am. Oil Chem. Soc. 88 (2011) 223–233, http://dx.doi.org/10.1007/s11746-010-1665-z.
[4] M. Teles dos Santos, V. Gerbaud, G.A.C. Le Roux, Simulation of chemical interesterification and melting curves for vegetable oils blends, in: 9th Euro Fed Lipid Congress, Rotterdam 2011: Lecture Abstracts, Eur. J. Lipid Sci. Technol. 113 (S1) (2011) 1–46, http://dx.doi.org/10.1002/ejlt.201100363.
[5] J.W. Prausnitz, R.N. Lichtenthaler, G.E. de Azevedo, Molecular Thermodynamics of Fluid Phase Equilibria, 3rd edition, Prentice-Hall, New York, 1998.

[6] L.H. Wesdorp, et al., Liquid-multiple solid phase equilibria in fats: theory and experiments, in: A.G. Marangoni (Ed.), Fat Crystal Networks, Marcel Dekker, New York, 2005, pp. 481–709.
[7] C.K. Zéberg-Mikkelsen, E.H. Stenby, Predicting the melting points and the enthalpies of fusion of saturated triglycerides by a group contribution method, Fluid Phase Equilib. 162 (1999) 7–17.
[8] R.E. Rosenthal, GAMS Release 23.2. A User's Guide, GAMS Development Corporation, Washington, DC, 2008.
[9] C.P. Tan, Y.B. Che Man, Differential scanning calorimetric analysis of edible oils: comparison of thermal properties and chemical composition, J. Am. Oil Chem. Soc. 77 (2000) 2, 143–155.
[10] R. Sambanthamurthi, K. Sundram, Y.-A. Tan, Chemistry and biochemistry of palm oil, Prog. Lipid Res. 39 (6) (2000) 507–558.
[11] R.D. O'Brien, Fats and Oils – Formulating and Processing for Applications, 2nd edition, CRC Press, 2003.
[12] K. Sato, S. Ueno, Crystallization transformation and microstructures of polymorphic fats in colloidal dispersion states, Curr. Opin. Colloid Interface Sci. 16 (2011) 384–390.
[13] C.P. Tan, Y.B. Che Man, Differential scanning calorimetric analysis of palm oil, palm oil based products and coconut oil: effects of scanning rate variation, Food Chem. 76 (1) (2002) 89–102.